Title
Implementation of a new scanning method for high-resolution fluorescence tomography using thermo-sensitive fluorescent agents.

Journal
Optics Letters, 40(21)

ISSN
0146-9592

Authors
Nouizi, Farouk
Kwong, Tiffany C
Cho, Jaedu
et al.

Publication Date
2015-11-01

DOI
10.1364/ol.40.004991

Peer reviewed

HHS Public Access

Author manuscript

Opt Lett. Author manuscript; available in PMC 2016 June 02.

Published in final edited form as:

Opt Lett. 2015 November 1; 40(21): 4991–4994.

Implementation of a new scanning method for high-resolution fluorescence tomography using thermo-sensitive fluorescent agents

Farouk Nouizi[1,*], **Tiffany C. Kwong**[1], **Jaedu Cho**[1], **Yuting Lin**[1,3], **Uma Sampathkumaran**[2], and **Gultekin Gulsen**[1]

[1]Tu and Yuen Center for Functional Onco-Imaging, Department of Radiological Sciences, Department of Biomedical Engineering, University of California, Irvine, California 92697, USA

[2]InnoSense LLC, 2531 West 237th Street, Suite 12, Torrance, California 90505, USA

[3]Department of Radiation Oncology, Massachusetts General Hospital and Harvard Medical School, Boston, Massachusetts 02114, USA

Abstract

Conventional fluorescence tomography provides images of the distribution of fluorescent agents within highly scattering media, but suffers from poor spatial resolution. Previously, we introduced a new method termed “temperature-modulated fluorescence tomography” (TM-FT) that generates fluorescence images with high spatial resolution. TM-FT first uses focused ultrasound to locate the distribution of temperature-sensitive fluorescence probes. Afterward, this *a priori* information is utilized to improve the performance of the inverse solver for conventional fluorescence tomography and reveal quantitatively accurate fluorophore concentration maps. However, the disadvantage of this novel method is the long data acquisition time as the ultrasound beam was scanned in a step-and-shoot mode. In this Letter, we present a new, fast scanning method that reduces the imaging time 40 fold. By continuously scanning the ultrasound beam over a 50 mm by 25 mm field-of-view, high-resolution fluorescence images are obtained in less than 29 min, which is critical for *in vivo* small animal imaging.

As an emerging molecular imaging modality, fluorescence tomography (FT) can provide 3D distributions of fluorescent agents *in vivo* using nonionizing radiation and low-cost instrumentation [1–4]. However, strong tissue scattering and the ill-posed inverse problem are the primary factors for the poor spatial resolution and low quantitative accuracy of this imaging technique [2]. The FT inverse problem is modeled by a linear integral equation when the fluorescence is assumed to be weak [5]. Meanwhile, high sensitivity of the solution to the noise in the measurements necessitates the utilization of regularization methods. Indeed, regularization is more efficient when spatial *a priori* information obtained from a structural imaging modality, such as MRI or X-ray CT, is integrated into the inverse problem formulation [6,7]. However, this approach fails if the boundary of the target delineated by the anatomic imaging modality does not overlap with the actual location of fluorophore.

*Corresponding author: ; Email: fnouizi@uci.edu

In a previous work, our team introduced a high-resolution fluorescence tomography technique called temperature-modulated fluorescence tomography (TM-FT) [8,9]. There are two key elements in this novel technique. The first is the high-intensity focused ultrasound (HIFU) that is used in a low power mode to heat the medium with high spatial resolution. The second is the recently emerged thermo-reversible fluorescence contrast agents (ThermoDots) consisting of ICG loaded pluronic nanocapsules [10,11]. The quantum efficiency and lifetime of these ThermoDots are extremely sensitive to slight temperature variations [9]. TM-FT is based on the monitoring of the temperature dependence of these ThermoDots during the low power HIFU scanning throughout the medium. Accordingly, TM-FT provides fluorescence images with much higher spatial resolution than conventional FT by using *a priori* binary location information provided by the temperature modulation of the ThermoDots (i.e., using them as binary switches). In this approach, first a conventional low resolution FT image is reconstructed to define a region of interest (ROI) around the target. Then, a focused ultrasound column is scanned over this ROI while monitoring the change in the fluorescence signal using selected FT source-detector pairs. This procedure localizes the ThermoDots at focused ultrasound resolution (~1.33 mm) and creates a binary map of the fluorophore distribution. Finally, the boundary of the fluorescent target outlined by this procedure is used as *a priori* information to recover quantitatively accurate concentration and lifetime images using the conventional FT data [9].

Unlike structural *a priori* information which reveals the boundaries of anatomic structures, this method directly delineates the boundary of the fluorescent target. Therefore, it is important to note that the TM-FT binary mask alone reveals a high-resolution image of the fluorescent agent distribution prior to any complex reconstruction process. However, recovering quantitative fluorescence concentration and lifetime parameters requires solving the inverse problem of FT. Our previous results demonstrated the superior performance of TM-FT compared to conventional FT. However, data acquisition time was the main weakness of this technique due to utilization of the HIFU step-and-shoot mode [8]. In this Letter, we introduce a fast scan method that drastically accelerates the acquisition speed without sacrificing the spatial resolution of this imaging technique. These preliminary experimental results show the ability of our fast scan TM-FT method to resolve small fluorescent inclusions embedded several centimeters deep in a scattering medium.

In general, the fluorescence signal measured at the surface of the imaged medium is independent from its temperature when using a conventional fluorescent agent. However, in our technique, the quantum efficiency of the ThermoDots is temperature dependent. The density of the fluorescence photons Φ_m within the medium at a temperature T is given by

$$\begin{cases} -\nabla[D_x\nabla\Phi_x] - [\mu_{af}+\mu_{ax}]\Phi_x = -q_0, \\ -\nabla[D_m\nabla\Phi_m(\eta(T))] - \mu_{am}\Phi_m(\eta(T)) = -\Phi_x\eta(T)\mu_{af}, \end{cases} \quad (1)$$

where q_0 is the source of excitation light. D and μ_a are the diffusion and absorption coefficients, respectively. Φ is the density of photons. The subscripts x, m represent the excitation and emission wavelengths, respectively. $\eta(T)$ is the temperature dependent fluorescence quantum yield, and μ_{af} is the fluorescence absorption.

Our TM-FT imaging system is mainly composed of two parts. The first is a conventional frequency-domain fluorescence tomography scanner using a 785 nm laser diode (300 mW). A multi-channel fiber-optic switch is used to deliver the 785 nm excitation light into one of the six source fibers illuminating the phantom. The transmitted light collected by six optical fibers is first filtered using two cascaded band-pass filters (830 nm) before being guided to a photomultiplier tube (R9880U-20 Hamamatsu). Once amplified by the RF amplifiers, the data are recorded with a network analyzer, which also provides a 100 MHz RF-modulation signal for the laser diode. The second part of our system consists of a HIFU transducer (H102, Sonic Concepts, Inc., WA) with a center frequency of 1.0 MHz. The transducer is driven by a sinusoidal signal generated by a functional generator and amplified by a power amplifier. Finally, to perform spatial scanning, the transducer is mounted on a computer controlled xy translational stages and placed above the phantom to be imaged.

The phantom used in this Letter is a 100(x) × 40(y) × 100 mm(z) agarose phantom. Its absorption and reduced scattering coefficients are set to 0.008 and 0.86 mm^{-1}, respectively. A 3 mm diameter, 10 mm long cylindrical inclusion filled with ThermoDots is embedded at the center of the phantom along the z-axis, 50 mm below the top surface (Fig. 1). The ThermoDot concentration used in this Letter generates a fluorescence signal equivalent to 0.8 μM of ICG at low temperature.

The previous step-and-shot technique requires more than an hour to scan an 8 × 8 mm ROI. In this Letter, the imaging time is considerably reduced by keeping the HIFU on continuously at low power, while scanning in both x and y directions [Fig. 1(b)]. Considering the size of the HIFU hot spot (~1.33 mm), 37 scanning lines cover an area of 49.21 × 25 mm^2 for the X-scan, while 18 scanning lines cover an area of 50 × 23.94 mm^2 for the Y-scan. The centers of both scanned areas are aligned at the center of the phantom.

While HIFU is generally used therapeutically at high power to burn tissue, here it is used diagnostically in a low power mode to induce a slight temperature change to generate a measurable increase in fluorescence signal [10]. However, the thermal diffusion and the effect of residual heat still needs to be taken into account. A typical thermal diffusivity value for most soft tissues is 14 × 10^{-4} cm^2/s [12]. The thermal diffusion length during the pulse period can be estimated by the following equation: $\delta_T = 2\sqrt{D_T \cdot \tau_p}$, where D_T is the thermal diffusivity and τ_p is the pulse width. Using this equation, the calculated thermal diffusion length for a one second pulse is 0.75 mm. For this reason, during a line scan, the HIFU beam is scanned faster, with a speed of 4.16 mm/s, to prevent the effect of heat diffusion from the portion of the line previously scanned. The network analyzer acquires 200 measurements in a 50 mm line scan yielding a sampling rate of one measurement per 0.25 mm. Thus, considering the size of the hot spot of the HIFU (1.33 mm), a filtering window width of five data points is used to smooth the measured signals.

We assign $\Phi_{PP'}$ to be the fluorescence signal measured while performing a linear scan from the point P to the point P', where P represents a particular scanning line denoted by letters A to E according to their scan sequence (Fig. 1). Meanwhile, $\phi_{PP'}$ represents the first derivative of $\Phi_{PP'}$. In the absence of ThermoDots along the scanning line, no change in the fluorescence signal is induced by the HIFU ($\Phi_{BB'}$) (Fig. 2). However, a sudden jump in the

fluorescence signal is detected when the HIFU is scanned over the target ($\Phi_{AA'}$) (Fig. 2). As soon as the HIFU beam leaves the target, the fluorescence signal starts decreasing at a lower rate due to cooling. Hence, the first derivative of the signal can only be used to identify the first encountered boundary of the fluorescence target ($\phi_{AA'}$). Therefore, a second scan is performed in the opposite direction ($\Phi_{A'A}$), and its derivative ($\phi_{A'A}$) is used to identify the boundary of the target from the opposite side. Each of these four scans is achieved in just over 7 min, which makes the total HIFU scanning time approximately 29 min. We observed that ζ_A, the sum of the derivatives obtained on line AA' in opposite directions ($\phi_{AA'}$ and $\phi_{A'A}$), reveals the boundaries of the inclusion on that particular line (Fig. 2). An interleaved scanning pattern is used to avoid waiting for the signal to decrease to the baseline before performing the scan in the opposite direction or crosstalk due to the heat diffusion in adjacent lines. While performing the Y-scans, the HIFU is sequentially scanned from point A to A', B' to B, C to C', and then A' to A… etc. [Fig. 1(b)]. A 2D image I_Y can be formed over the Y-scan by assembling all the sums (ζ_A, ζ_B, ζ_C, …) with respect to their spatial coordinates [Fig. 3(b)]. Similarly, I_X can be formed over the X-scan [Fig. 3(a)].

An elongation in the shape of the inclusion is indeed noticed along the scanning direction, y-axis for I_X and x-axis for I_Y [Figs. 3(a) and 3(b)]. Figure 3(c) shows the image I_{XY} resulting from the product pixel to pixel of I_X and I_Y. It demonstrates that the circular shape of the target is recovered better using a combination of both scans I_X and I_Y. This correction of the target shape is clearly observed by the full width at half-maximum (FWHM) values of the profiles of I_X, I_Y, and I_{XY} along both the x- and y-axis, across the target given at the top of each individual map in Fig. 3. They show that each scan improves the spatial resolution of the final image in its orthogonal direction. The binary mask used as *a priori* information to constrain the FT reconstruction algorithm is obtained by simply segmenting the I_{XY} at half-maximum [10].

In the first experiment, the 3 mm diameter inclusion is shifted by 6 mm to the left of the center of the phantom. A very good agreement is obtained between the mask generated using our new, fast TM-FT method and the real inclusion size and position [Figs. 4(a) and 4(b)]. The irregularities on the shape of the inclusion are only due to the interpolation of the segmented I_{XY} on the FEM mesh. Furthermore, the TM-FT method [Fig. 4(d)] recovers the object better than conventional FT, where no *a priori* information is used [Fig. 4(c)]. In fact, conventional FT recovered the size of the target more than four times its original size [Figs. 4(e) and 4(f)]. However, our method accurately localized the target size and position. Moreover, TM-FT recovered the fluorescence absorption with high quantitative accuracy with less than 3% error.

Next, a second identical target is embedded to test the limits of our method in distinguishing two nearby inclusions. The minimum distance between the two inclusions successfully resolved by our method is ~1.4 mm [Fig. 5(a)]. This distance is approximately equal to the size of the hot spot of our HIFU (~1.33 mm). Figure 5(c) shows that conventional FT completely fails to resolve the two inclusions. On the other hand, the TM-FT mask represents a high-resolution distribution of the fluorophore prior to any reconstruction process [Fig. 5(b)]. Using this mask, TM-FT is able to resolve both targets successfully [Fig. 5(d)]. Moreover, TM-FT overestimates the fluorescence absorption by only ~9%, while

conventional FT underestimates it by more than 90%. This small quantitative error of TM-FT is due to the slight underestimation of the target size in the mask (2.87 mm) [Fig. 5(f)]. The improvement in the spatial resolution is clearly visible on the profiles carried out along the inclusions [Figs. 5(e) and 5(f)]. In fact, despite the limited source-detector configuration, the spatial resolution is improved not only in the x-axis, but also along the y-axis.

In conclusion, we have demonstrated a new continuous-scan approach that drastically reduces the TM-FT imaging time. This opens the possibility for high-resolution whole-body *in vivo* small animal imaging as this continuous scanning method can image a field-of-view of 50 × 25 mm in less than 29 min and, hence, reduces the overall imaging time 40 fold compared to the previous step-and-shot mode. Please note that this time reduction is obtained by sacrificing the sensitivity since performing derivative reduces the overall signal to noise ratio by six times for this particular experimental setting. As for any imaging modality, the performance of TM-FT degrades when background fluorescence is present. However, using targeted ThermoDots has the potential to alleviate this effect by selectively accumulating in diseased tissue and increase the performance of TM-FT.

Acknowledgments

Funding. Fulbright Commission (Visiting Scholar); National Institutes of Health (NIH) (F31CA17191501A1, P30CA062203, R01EB008716, R21CA191389, R21EB013387, SBIRHHSN261201300068C).

REFERENCES

1. Graves EE, Yessayan D, Turner G, Weissleder R, Ntziachristos V. J. Biomed. Opt. 2005; 10:44019. [PubMed: 16178652]
2. Leblond F, Davis SC, Valdes PA, Pogue BW. J. Photochem. Photobiol. B. 2010; 98:77. [PubMed: 20031443]
3. Ntziachristos V. Annu. Rev. Biomed. Eng. 2006; 8:1. [PubMed: 16834550]
4. Sevick-Muraca EM, Rasmussen JC. J. Biomed. Opt. 2008; 13:041303. [PubMed: 19021311]
5. Ntziachristos V, Weissleder R. Opt. Lett. 2001; 26:893. [PubMed: 18040483]
6. Davis SC, Dehghani H, Wang J, Jiang S, Pogue BW, Paulsen KD. Opt. Express. 2007; 15:4066. [PubMed: 19532650]
7. Lin Y, Yan H, Nalcioglu O, Gulsen G. Appl. Opt. 2009; 48:1328. [PubMed: 19252634]
8. Lin Y, Bolisay L, Ghijsen M, Kwong TC, Gulsen G. Appl. Phys. Lett. 2012; 100:73702. [PubMed: 22393266]
9. Lin Y, Kwong TC, Bolisay L, Gulsen G. J. Biomed. Opt. 2012; 17:056007. [PubMed: 22612130]
10. Chen Y, Li X. Biomacromolecules. 2011; 12:4367. [PubMed: 22040128]
11. Kim TH, Chen Y, Mount CW, Gombotz WR, Li X, Pun SH. Pharm. Res. 2010; 27:1900. [PubMed: 20568000]
12. McKenzie AL. Phys. Med. Biol. 1990; 35:1175. [PubMed: 2236204]

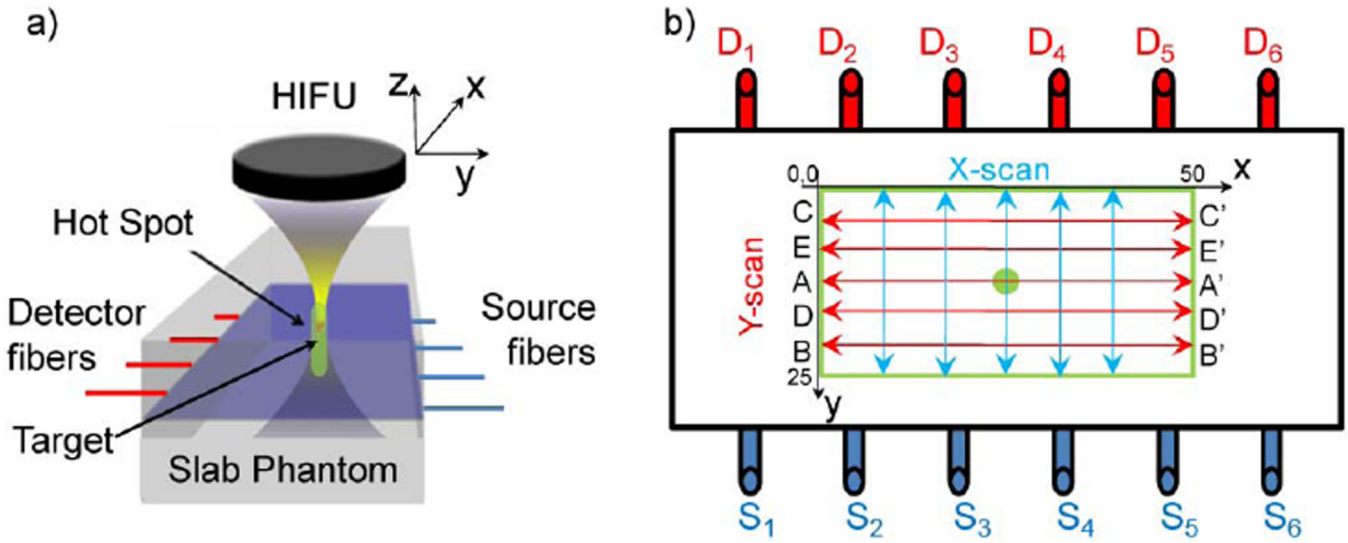

Fig. 1.

(a) HIFU transducer is positioned at the top of the agar phantom while six source (blue) and six detector (red) fibers are placed at both sides of the phantom. (b) Cross section of the phantom at the fiber plane, 50 mm below the top surface [the blue plane in (a)]. HIFU beam is scanned in two orthogonal directions, X-scan (blue) and Y-scan (red), over the phantom (bold black). The cylindrical fluorescent target is positioned at the center of the phantom along the z-axis.

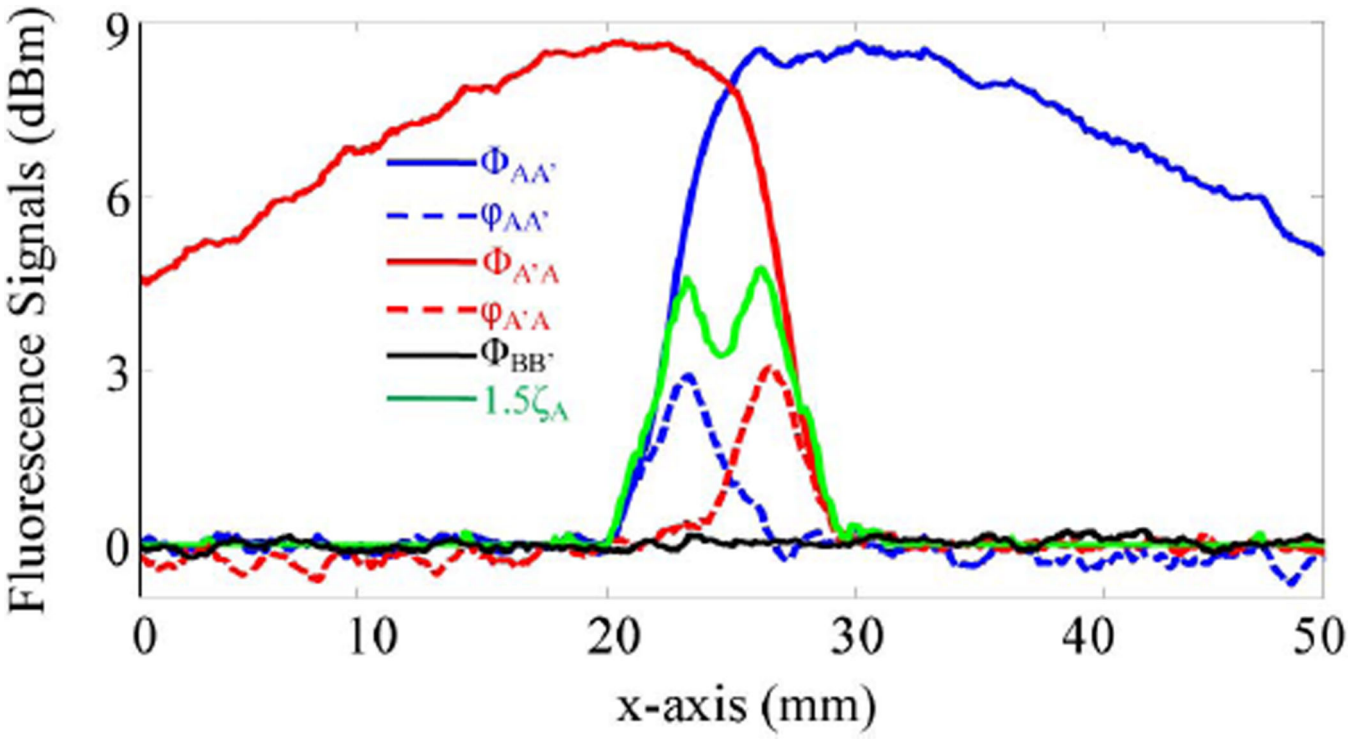

Fig. 2.

Measured fluorescence signals on a single Y-scan (AA') in opposite directions (blue and red solid lines) for the phantom with single target. The derivatives (blue and red dashed lines) reveal the boundaries of the target for this particular Y-scan (AA') when summed together (green solid line).

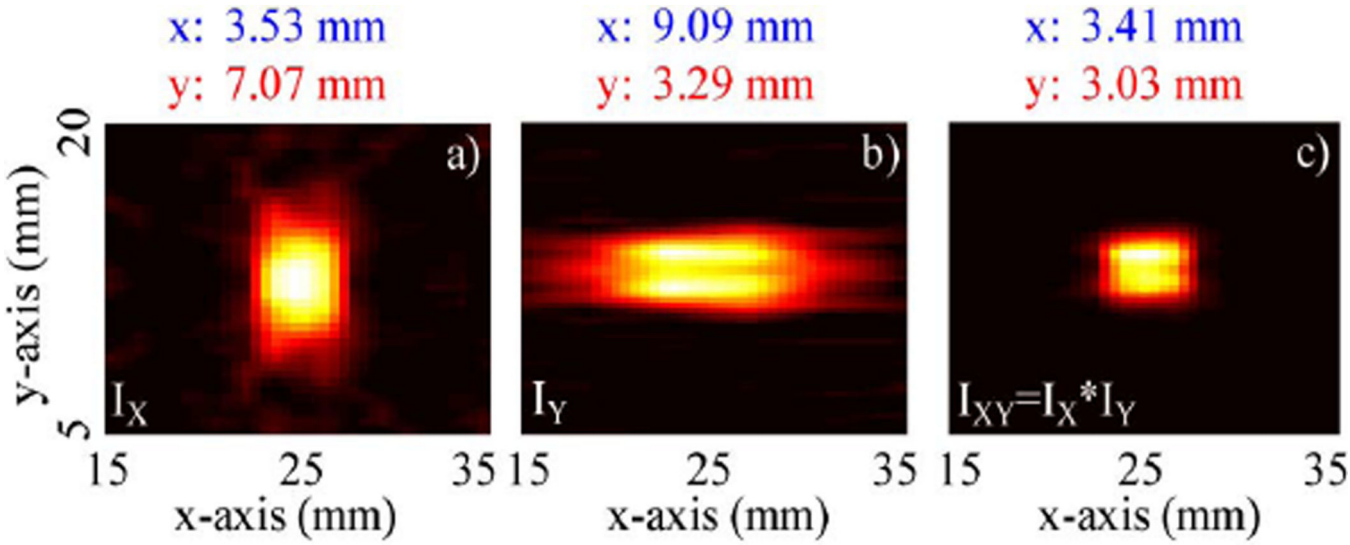

Fig. 3.

Assembling the sum of the derivatives for all of the lines provides the approximate location and shape of the target, I_X (a) and I_Y (b). However, combination of these maps obtained by the product of X- and Y-scans provides a better extraction of the real boundary of the fluorescence target, I_{XY} (c). The FWHM values along the x- and y-directions are provided above.

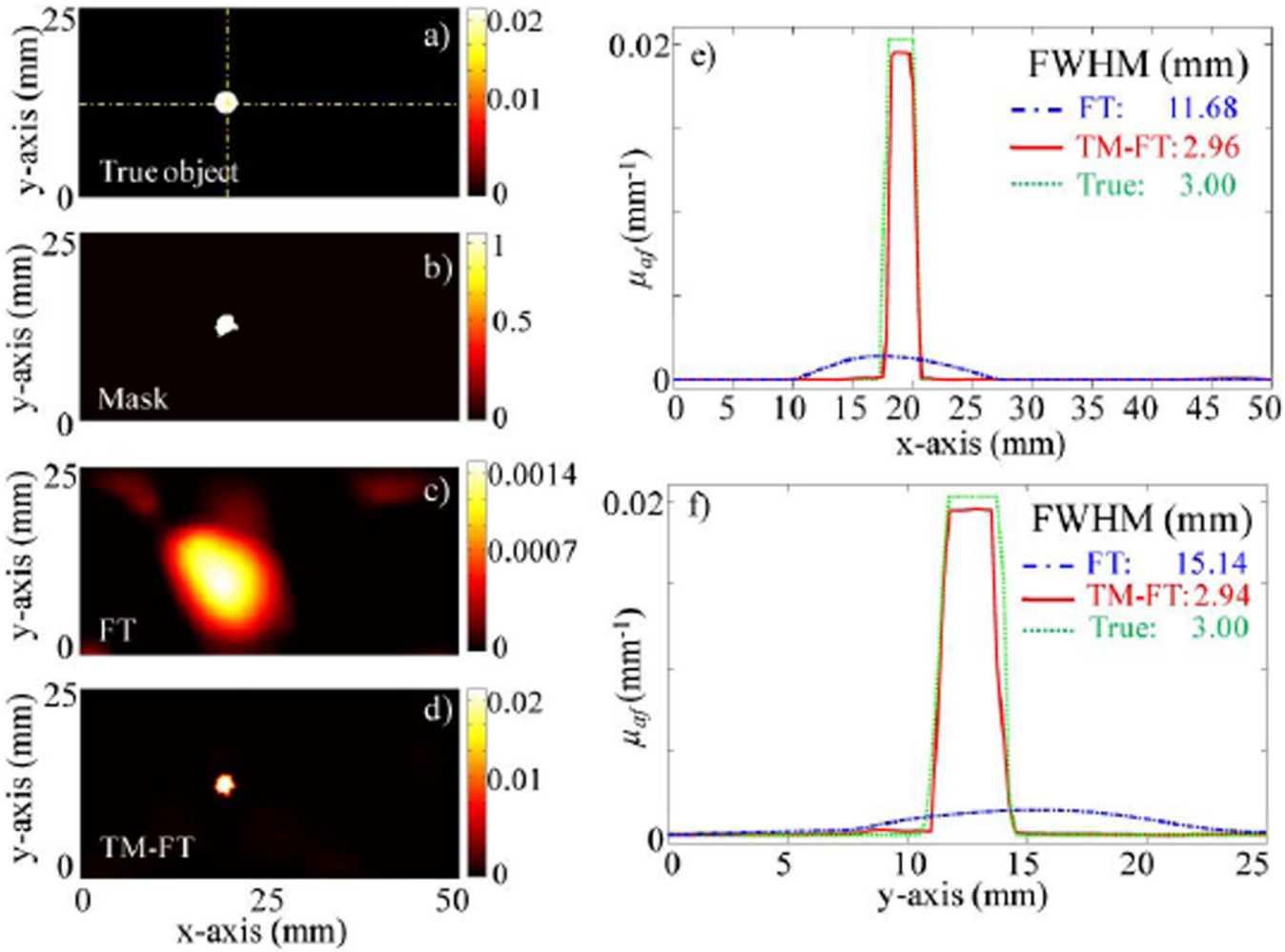

Fig. 4.

Experiment results for the first phantom with a single 3 mm diameter target. (a) True ThermoDot distribution in the optical fiber plane. (b) Binary map obtained using TM-FT. (c) Reconstructed fluorescence map using conventional FT with no *a priori* information. (d) Reconstructed fluorescence map using TM-FT. The profiles across the fluorescence target along (e) x- and (f) y-directions show that the size of the fluorescence target is accurately recovered.

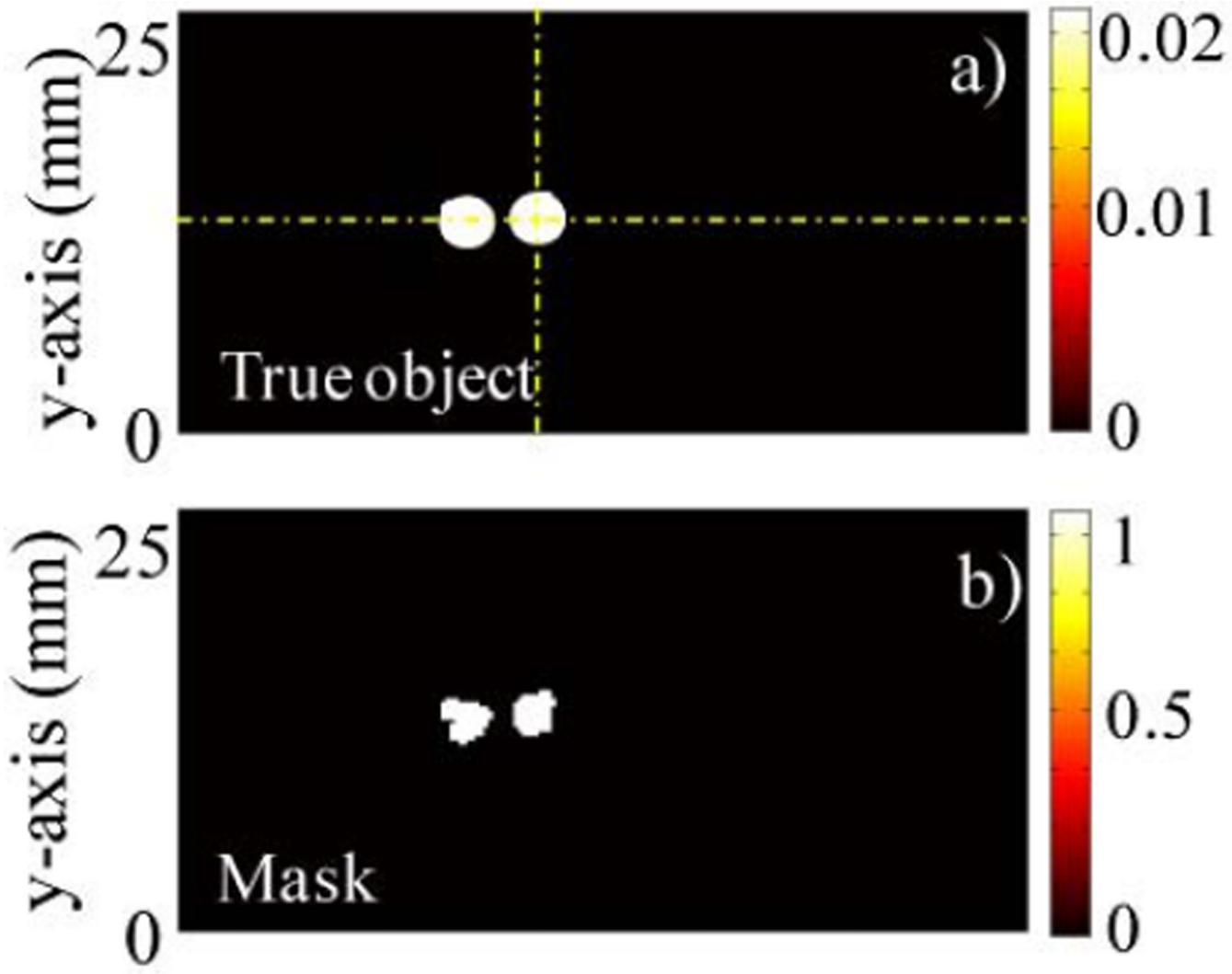

Fig. 5.

Experiment results for the second phantom with two identical targets separated by 1.4 mm. (a) True ThermoDot distribution in the optical fiber plane. (b) Binary map obtained using TM-FT. (c) Reconstructed fluorescence map using conventional FT with no *a priori* information. (d) Reconstructed fluorescence map using TM-FT. The profiles along the dashed yellow lines (e) x- and (f) y-directions show that the sizes of the fluorescence targets are accurately recovered.